

Surprising stability of polar (001) surfaces of the Mott insulator GdTiO_3

Cite as: J. Vac. Sci. Technol. A 39, 063220 (2021); doi: 10.1116/6.0001313

Submitted: 25 July 2021 · Accepted: 5 October 2021 ·

Published Online: 1 November 2021



Karthik Krishnaswamy,¹ Anderson Janotti,² Lars Bjaalie,³ and Chris G. Van de Walle³

AFFILIATIONS

¹Department of Electrical and Computer Engineering, University of California, Santa Barbara, California 93106-9560

²Department of Materials Science and Engineering, University of Delaware, Newark, Delaware 19716-3106

³Materials Department, University of California, Santa Barbara, California 93106-5050

Note: This paper is a part of the Special Collection Honoring Dr. Scott Chambers' 70th Birthday and His Leadership in the Science and Technology of Oxide Thin Films.

ABSTRACT

Using first-principles techniques based on hybrid density functional calculations, we study the stability, energetics, and electronic structure of the (001) surface of the Mott insulator GdTiO_3 (GTO), which has an orthorhombic perovskite structure. Interestingly, we find the bare unreconstructed (but relaxed) polar surface terminated by a TiO_2 plane to be very stable with a low surface energy ($71 \text{ meV}/\text{\AA}^2$). As a test for stability of the TiO_2 termination against reconstructions, we studied the influence of an H adatom. Hydrogen is known to form strong bonds with surface O atoms and passivate surface states, but contrary to expectations, hydrogen does not lead to a lowering of the GTO surface energy. We explain the energetics based on the surface electronic structure. We also address the interaction between the TiO_2 -terminated GTO surface and the high-density two-dimensional electron gas (2DEG) that can be formed at an SrTiO_3 (STO)/GTO heterointerface. Unlike the situation in STO/ LaAlO_3 (LAO) heterostructures, where the LAO surface acts as a sink for electrons, the GTO surface does not drain electrons away from the 2DEG.

Published under an exclusive license by the AVS. <https://doi.org/10.1116/6.0001313>

I. INTRODUCTION

Surfaces have a strong influence on growth and on electronic properties of heterostructures and semiconductor devices. Compared to conventional semiconductors, surfaces of complex oxides have received far less attention to date, in spite of the fact that they are known to play a crucial role in determining the electronic properties of complex oxide heterostructures. One example is the high-density two-dimensional electron gas (2DEG) at the $\text{SrTiO}_3/\text{LaAlO}_3$ (STO/LAO) interface, where electron transfer to surface states of LAO depletes the 2DEG.¹⁻³ These complex oxides generally assume the perovskite structure, with the chemical formula ABO_3 , and exhibit a wide variety of electronic properties including ferromagnetism, ferroelectricity, superconductivity, and Mott insulating behavior.⁴ Their surface properties can be complex and challenging to probe using experimental techniques.^{5,6} First-principles calculations have proved valuable in building an understanding of the fundamental properties of these oxides;⁷⁻¹⁰ here, we will apply them to the study of surfaces.

GdTiO_3 (GTO) is an orthorhombic perovskite oxide ($Pnmb$ space group) (see Fig. 1) and a $3d^1$ ferromagnetic Mott insulator. The Mott-Hubbard gap is formed as a result of strong electron-electron interactions that split one of the Ti $3d$ bands into a fully occupied spin-up channel [the lower Hubbard band (LHB)], and an unoccupied spin-down channel [the upper Hubbard band (UHB)].^{9,11-13} The Ti atoms in GTO thus occur in a $3+$ valence state (Ti^{3+}), in contrast to the $4+$ state (Ti^{4+}) in, e.g., STO, which is a band insulator. The other valences are Gd^{3+} and O^{2-} . In an ionic picture, GTO can be viewed along the [001] direction as consisting of alternating planes of $(\text{TiO}_2)_2$ layers with a net charge of -2 per 1×1 areal unit (a 1×1 areal unit of GTO contains 2 formula units of TiO_2), and $(\text{GdO})_2$ layers with a net charge of $+2$ per 1×1 areal unit, as illustrated in Fig. 1(a). GTO is thus polar along the [001] direction. It should be kept in mind, though, that the ionic picture results from each of the GdO (*donorlike*) planes donating $1e^-$ per 1×1 areal unit (corresponding to an electron density of $3.3 \times 10^{14} \text{ cm}^{-2}$), to each of the two neighboring TiO_2 (*acceptorlike*) planes on either side.

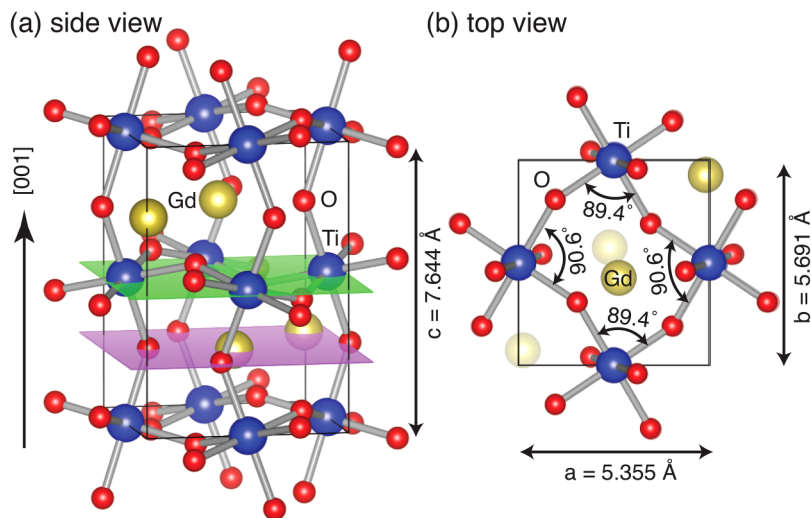


FIG. 1. (a) Side view of the structure, depicting its polar nature with alternating TiO_2 and GdO planes along the $[001]$ direction. (b) Top view of the (001) plane of the 20-atom distorted perovskite structure of GdTiO_3 , indicating lattice parameters and O–Ti–O bond angles.

At a (001) surface, the symmetry of this stacking sequence is broken. In the case of termination on a GdO plane, this results in a seeming excess of $1e^-$ per 1×1 areal unit (which would have been transferred to a TiO_2 plane that is now missing). In the case of TiO_2 termination, there is a seeming deficiency of $1e^-$ per 1×1 areal unit (due to a lack of electron transfer from a GdO plane that is now missing). Within an ionic picture, the charge imbalance is assumed to lead to unstable surfaces¹⁴ that require significant reconstructions or changes in stoichiometry to overcome the instability. We will show how, in the case of Mott insulators, such drastic rearrangements do not occur: the bare unreconstructed surfaces turn out to be remarkably stable.

To our knowledge, there have been no studies on the surface of Mott insulators except for an analysis of the Mott interaction in a model system for the surface of a simple cubic lattice using Dynamical Mean Field Theory (DMFT).¹⁵ One of the goals of the present work is to address the stability against reconstructions of polar surfaces of GTO and develop an understanding of the behavior of Mott insulator surfaces by linking energetics to electronic structure.

The electronic behavior of a polar surface, which is an interface with vacuum, is expected to be similar to that of a heterointerface with a nonpolar material. At an interface with STO (which is nonpolar along the $[001]$ direction), the GdO layer acts as a source of electrons that form a 2DEG with a density of $\sim 3.3 \times 10^{14} \text{ cm}^{-2}$ (based on the STO lattice constant of 3.905 Å).^{2,3,16} The underlying mechanism is the same as for an STO/LAO interface,^{1,2,17} where the donorlike LaO plane at the interface donates electrons to the conduction band of the nonpolar STO. The conduction-band offset between the nonpolar and polar materials ensures that the 2DEG is confined within the nonpolar material.^{9,18} While the mechanism of 2DEG formation is identical, the 2DEG densities reported for STO/LAO^{17,19} are much smaller than the expected density of $\sim 3.3 \times 10^{14} \text{ cm}^{-2}$ [which is actually observed for STO/GTO (Ref. 16)]. In addition, in the STO/LAO system, the formation of the 2DEG requires a critical thickness of LAO.^{17,20} These effects can be attributed to the proximity of the LAO surface to the 2DEG

at the STO/LAO interface, with the surface acting as a sink for electrons.^{2,3} It is still an open question why these effects are not observed for STO/GTO heterostructures. In the present work, we address how GTO surfaces interact with a nearby 2DEG at an STO/GTO heterointerface and compare the behavior of this system with that of the STO/LAO system.

Our goal in this paper is thus twofold: (1) to study the energetics and atomic and electronic structure of GTO polar surfaces and (2) to assess the influence of the GTO surface on the 2DEG in an STO/GTO heterostructure. We perform density functional theory (DFT) calculations using the hybrid functional by Heyd, Scuseria, and Ernzerhof (HSE06)^{21,22} on the two polar (001) terminations, namely, GdO and TiO_2 terminations. The use of hybrid functional is essential to capture the strong electron localization effects characteristic of a Mott insulator and to accurately describe the electronic structure of GTO, as was demonstrated in a recent joint theoretical/experimental study.¹⁰

GTO can be grown either along the $[001]_o$ or $[110]_o$ directions; the subscript “o” identifies the direction with respect to the orthorhombic unit cell, to distinguish it from directions defined for a pseudocubic cell (subscript “c”). $[001]_o$ and $[001]_c$ coincide, while $[110]_o$ corresponds to $\langle 001 \rangle_c$. $[001]_o$ and $[110]_o$ thus have equivalent atomic stacking sequences. However, since they are distinct in the orthorhombic crystal structure, they result in slightly different strains for a given substrate. Different growth orientations result in different strains with respect to the substrate lattice, e.g., on a $(\text{LaAlO}_3)_{0.3}(\text{Sr}_2\text{AlTaO}_6)_{0.7}$ substrate the $[110]_o$ direction results in a strain of -0.55% and the $[001]_o$ direction results in a strain of -1.61% .²³ For the purposes of our surface stability study, we focus on the $[001]_o$ orientation (which we simply refer to as $[001]$); however, our qualitative conclusions apply to the $[110]_o$ orientation as well.

Our calculations show that the polar unreconstructed (but relaxed) TiO_2 termination is quite stable with a low surface energy of $71 \text{ meV}/\text{\AA}^2$ under Ti-rich conditions. This high degree of stability is unexpected for the surface of a polar material, and we explain it based on the electronic structure of this Mott insulator. We also

address how surface modifications affect the stability. Hydrogen is known to passivate surfaces of many materials^{24,25} and is particularly expected to do so in oxides^{25–27} due to the formation of strong O–H bonds. Surprisingly, our calculations for H adatoms will show that they do not lower the surface energy of GTO; this behavior can, again, be understood based on the electronic structure and the nature of the bonding.

This paper is organized as follows: **Sec. II** presents our first-principles computational methodology to calculate the surface energies. **Section III A** contains results for the bulk properties of GTO. In **Sec. III B**, we discuss the atomic and electronic structure of the two polar terminations, while **Sec. III C** focuses on the stability based on the calculated surface energies. In **Sec. III D**, we discuss the surface energy in the presence of hydrogen. **Section III E**, finally, addresses the interaction between the GTO surface and the 2DEG at an STO/GTO interface.

II. COMPUTATIONAL METHODOLOGY

Our calculations of the bulk and surface properties rely on density functional theory utilizing the HSE06 hybrid functional^{21,22} with the default mixing parameter of 25% and screening parameter of 0.2 \AA^{-1} . This functional has been shown to yield accurate electronic structures for oxides.^{9,22,28,29} Specifically, for GTO, it correctly produces the value of the Mott–Hubbard gap, as compared with recent optical measurements.¹⁰ The calculations were performed using the Vienna *ab initio* Simulation Package³⁰ with projector augmented wave potentials³¹ and a plane-wave cutoff of 500 eV. Gd $6s^2 5p^6 5d^1$, Ti $4s^2 3d^2$, and O $2s^2 2p^4$ were treated as valence electrons in all of our calculations.

The surfaces are studied using a slab geometry with two identical surfaces separated by vacuum. Based on convergence tests for the slab thickness and vacuum thickness, we determined a slab with 13 layers (thickness $\sim 23 \text{ \AA}$) separated by $\sim 23 \text{ \AA}$ of vacuum to be sufficiently large to ensure convergence of surface energies. In the surface calculations, we relax the first four layers (two TiO_2 and two GdO layers) closest to each of the surfaces and keep the remaining 5 bulklike layers fixed to represent the bulk region. Relaxations were performed until forces on all the atoms were less than 0.05 eV/\AA . For Brillouin zone (BZ) integrations, we use a Monkhorst–Pack mesh of $4 \times 4 \times 2$ for the bulk calculations, and $4 \times 4 \times 1$ for the surfaces. All these choices were made to ensure that the surface energies are converged to within 1 meV/\AA^2 .

The surface energy for a given surface structure is computed based on the standard formalism established in **Ref. 32** using the total energy of the slab supercell E_{slab} as

$$\gamma_{\text{surface}} = \frac{1}{2} [E_{\text{slab}} - E_{\text{bulk}} - n_{\text{Gd}}[\mu_{\text{Gd}} + E_{\text{tot}}(\text{Gd})] - n_{\text{Ti}}[\mu_{\text{Ti}} + E_{\text{tot}}(\text{Ti})] - n_{\text{O}}[\mu_{\text{O}} + E_{\text{tot}}(\text{O})]], \quad (1)$$

where E_{bulk} is the total energy of a bulk supercell, n_i accounts for the number of atoms of species i in excess present in the surface supercell, and μ_i is the chemical potential referenced to the total energy $E_{\text{tot}}(i)$ of the bulk form of species i in our DFT calculation and represents the experimental growth conditions. The chemical potentials μ_i are discussed in more detail in **Sec. III A**.

III. RESULTS AND DISCUSSION

A. Bulk properties

The calculated lattice parameters for the 20-atom orthorhombic unit cell of GTO are: $a = 5.355 \text{ \AA}$, $b = 5.731 \text{ \AA}$, and $c = 7.644 \text{ \AA}$ (indicated in **Fig. 1**), in good agreement with the experimental values³³ of 5.393 \AA , 5.691 \AA , and 7.664 \AA . In order to discuss structural relaxations, we will use the O–Ti–O bond angles between atoms lying along the (001) plane as an indicator of distortions. It is important to note that we are not referring to angles between atomic positions *projected* on a plane but rather angles that take atomic positions in three dimensions (3D) into account. **Figure 1(b)** shows the O–Ti–O bond angles in the bulk, which are 89.4° and 90.6° , and happen to sum up to 360° . However, given the 3D nature of the structure, these O–Ti–O angles do not necessarily lie in a single plane, and, therefore, the sum is not geometrically constrained to the value for a quadrilateral, 360° .

In the electronic structure of bulk GTO, the completely filled LHB, containing $4e^-$ ($1e^-$ per Ti atom), is separated from the UHB by a direct gap of 2.08 eV at Γ , and an indirect gap of 2.03 eV between a point along Y–Z and Γ ; a full diagram of the band structure was given in **Ref. 10**. The bandwidth of the LHB is less than 0.56 eV . The occupied O-2p bands occur at 2.47 eV below the bottom of the LHB.

The chemical potentials μ_i introduced in **Eq. (1)** are related to each other via the phase stability equation for GTO, namely,

$$\mu_{\text{Gd}} + \mu_{\text{Ti}} + 3\mu_{\text{O}} = \Delta H_f(\text{GdTiO}_3), \quad (2)$$

where $\Delta H_f(\text{GdTiO}_3)$ is the enthalpy of formation of GTO. The range of values that μ_i can take is limited by the formation of other phases. For the elemental phases (Gd metal, Ti metal, and the O_2 molecule), the constraint is given by

$$\mu_i \leq 0, \quad (3)$$

where i is Gd, Ti, or O. The constraints imposed by the formation of competing phases are represented by the following inequality equations:

$$\mu_{\text{Ti}} + 2\mu_{\text{O}} \leq \Delta H_f(\text{TiO}_2), \quad (4)$$

$$2\mu_{\text{Gd}} + 3\mu_{\text{O}} \leq \Delta H_f(\text{Gd}_2\text{O}_3), \quad (5)$$

$$2\mu_{\text{Gd}} + 2\mu_{\text{Ti}} + 7\mu_{\text{O}} \leq \Delta H_f(\text{Gd}_2\text{Ti}_2\text{O}_7). \quad (6)$$

The calculated values for the enthalpy of formation of the competing phases are tabulated in **Table 1** along with that of GTO.

The combination of **Eqs. (2)–(6)** determines the range of allowed values for μ_{Gd} , μ_{Ti} , and μ_{O} within which GTO is stable. This range can be represented by the phase stability diagram in **Fig. 2**, plotted as a function of μ_{Ti} and μ_{O} , where μ_{Gd} can be obtained from **Eq. (2)**. We note that the stability region for GdTiO_3 is identical to that reported in **Fig. 2** of **Ref. 37**. In addition, in **Fig. 2**, we indicate the stability region of the other competing phases. From the diagram, the boundary between GTO and TiO_2

TABLE I. Enthalpy of formation (ΔH_f), in units of eV/(formula unit), for GdTiO_3 and its competing phases.

Material	Enthalpy of formation ΔH_f	
	Calculated	Experimental
GdTiO_3	-17.20	—
Gd_2O_3	-18.68	-18.85 (Ref. 34)
TiO_2	-9.16	-9.74 (Ref. 35)
$\text{Gd}_2\text{Ti}_2\text{O}_7$	-38.02	-39.62 (Ref. 36)

represents the most Ti-rich conditions for GTO, while the boundary between GTO and Gd_2O_3 represents the most Gd-rich conditions. We also see that μ_{O} is restricted to $-5.24 \text{ eV} \leq \mu_{\text{O}} \leq -3.62 \text{ eV}$ for Gd-rich, and $-4.58 \text{ eV} \leq \mu_{\text{O}} \leq -3.62 \text{ eV}$ for Ti-rich conditions, due to the formation of $\text{Gd}_2\text{Ti}_2\text{O}_7$ and Ti metal ($\mu_{\text{Ti}} > 0 \text{ eV}$). These restrictions on μ_{O} determine the O-poor (most negative μ_{O}) and O-rich (least negative μ_{O}) limits under Gd-rich or Ti-rich conditions. These limiting values of μ_{O} are consistent with the growth conditions by hybrid molecular beam epitaxy in Ref. 23 that correspond to extremely low O_2 gas partial pressures due to their only source of O_2 being the metal-organic precursor. We will discuss the calculated surface energies in the Ti-rich as well as the Gd-rich conditions while varying μ_{O} between O-poor and O-rich limits.

B. Surface atomic and electronic structure

The electronic band structure for the surfaces is shown in Fig. 3. It includes the two-dimensional (2D) band structure of the

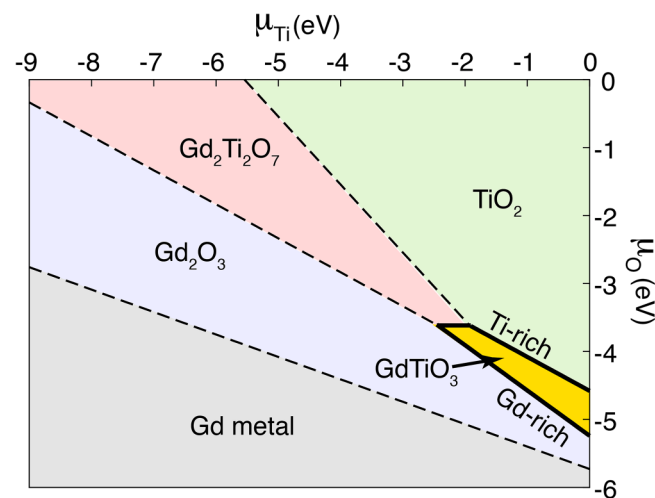


FIG. 2. Stability region of GdTiO_3 (yellow region enclosed by solid lines) as a function of μ_{Ti} and μ_{O} . Regions of stability of competing phases ($\text{Gd}_2\text{Ti}_2\text{O}_7$, Gd_2O_3 , and TiO_2) are also shown. The phase boundary of GdTiO_3 with Gd_2O_3 is indicated as Gd-rich, while the boundary with TiO_2 is indicated as Ti-rich. Note that due to the additional 0.5 O per Gd, the Gd-rich and Ti-rich boundaries for the $\text{Gd}_2\text{Ti}_2\text{O}_7$ phase have different slopes compared to boundaries of GdTiO_3 .

slab supercell along with a projection of the three-dimensional (3D) bulk band structure onto the 2D BZ. The perturbation due to the surface termination can introduce surface states, which are characterized by their charge density being localized on the surface layers. By plotting and visualizing the charge density for the states appearing in the gap, we explicitly verified that they are indeed surface states. The unreconstructed (yet relaxed) TiO_2 -terminated surface [Fig. 3(a)] shows an occupied surface state close to the LHB, and unoccupied surface states within the Mott–Hubbard gap at an energy $> 1.2 \text{ eV}$ above the LHB. We find that the highest occupied state is localized on one of the surface Ti atoms; this Ti atom assumes a 3+ valence, i.e., the same as in the bulk of the Mott insulator, a LHB-like state. As discussed in the Introduction, for the TiO_2 termination, there is a seeming deficit of $1e^-$ per (1×1) areal unit cell in the surface layer, compared to the number of electrons that would be available in the bulk. This deficit results in one of the Ti atoms in the surface layer being converted from Ti^{3+} to Ti^{4+} and the appearance of unoccupied surface states. The lowest unoccupied state occurs on the surface Ti atom, that is, in a 4+ valence. The two Ti atoms are labeled Ti^{3+} and Ti^{4+} in Fig. 4(a). The atomic structure shows that the in-plane O–Ti–O bond angles differ significantly from the bulk values: the unoccupied Ti^{4+} atom has the angles 94.0° and 81.9° , and the occupied Ti^{3+} has 97.9° and 86.2° , as shown in Fig. 4(a); the sum of the angles is still 360° .

The absolute position of the top of the LHB, i.e., referenced to the vacuum level, is -3.94 eV [Fig. 3(a)]. This is rather close to the vacuum level. In other oxides, in which the valence-band

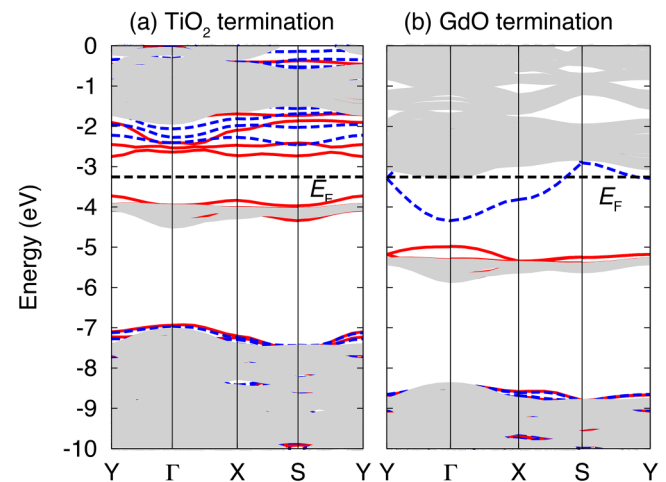


FIG. 3. Surface band structure of (a) TiO_2 -terminated and (b) GdO -terminated GTO projected onto the 2D (001) Brillouin zone. The gray regions are bulk states projected onto the 2D surface BZ. The solid (red) lines represent the spin-up (majority spin) channel of the surface supercell, while dashed (blue) lines represent the spin-down (minority spin) channel. For the metallic GdO termination, the Fermi level (E_F) is determined based on the occupation of states in the slab supercell calculations; for the insulating TiO_2 termination, E_F is set midway between the highest occupied and lowest unoccupied. The fact that the Fermi level appears at the same energy for the two terminations is a coincidence. The zero of energy is set to the vacuum level.

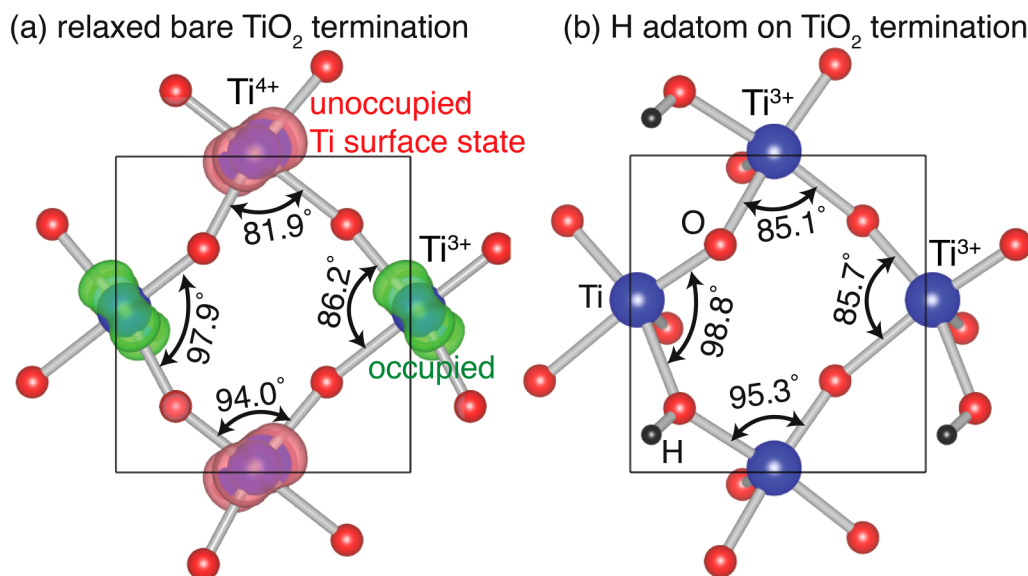


FIG. 4. Atomic structure of the GTO [001] surface with TiO_2 termination for (a) the bare unreconstructed (but relaxed) surface and (b) the H-adatom reconstruction. In-plane O–Ti–O bond angles are indicated. Iso-surfaces are shown for the charge densities of the highest occupied (in green; see label “occupied”) and lowest unoccupied (in red; see label “unoccupied Ti surface state”) surface states of the bare termination. The valence of the Ti atoms is also indicated.

maximum is derived from O $2p$ orbitals, the highest occupied level typically lies 6.5–7.5 eV below the vacuum level.^{3,38} The *unoccupied* surface states occurring > 1.2 eV above the LHB thus lie at > -2.74 eV on an absolute scale. The GdO termination shows a distinctly different behavior. It is expected to have an *excess* of $1e^-$ per (1×1) areal unit. The electronic band structure in Fig. 3(b) indeed shows an occupied surface state in the upper part of the gap. This state is found to have Gd $5d$ orbital character, explaining why it is less localized and more dispersive than states derived from Ti $3d$ orbitals. For the GdO termination, the calculated position of the top of the LHB is 5.29 eV below the vacuum level. This leads to a difference of 1.35 eV in the absolute position of the maximum of the LHB between the two polar terminations, with the GdO termination having the lower position. The Fermi level E_F for the GdO termination is at 3.22 eV below the vacuum level.

C. Stability

We now examine the stability of different surface terminations, based on the surface energies calculated using Eq. (1), as plotted in Fig. 5 for Gd-rich versus Ti-rich conditions. The fact that the surface energies are independent of μ_O under Ti-rich conditions is a consequence of the surface stoichiometry, which cancels out the variable μ_O in Eq. (1) due to the limiting phase being TiO_2 . Gd-rich conditions, on the other hand, introduce a μ_O -dependence in the surface energy due to the limiting phase being Gd_2O_3 .

Under Ti-rich conditions [Fig. 5(a)], the surface energy of the TiO_2 termination is $71 \text{ meV}/\text{\AA}^2$ for all μ_O . Under the same conditions, the GdO termination has a surface energy of $125 \text{ meV}/\text{\AA}^2$, considerably higher (i.e., less stable) than the TiO_2 termination. Under Gd-rich conditions [Fig. 5(b)], the TiO_2 termination has a

lower surface energy than the GdO termination for $\mu_O > -4.26$ eV, while for lower oxygen chemical potentials ($\mu_O < -4.26$ eV), the GdO termination is favored. The fact that the GdO termination would be favorable under Gd-rich conditions is not surprising but the TiO_2 termination is remarkably stable under both Ti-rich and Gd-rich conditions. For comparison, surface energies of silicon are above $85 \text{ meV}/\text{\AA}^2$ (Ref. 39). For LAO, the unreconstructed AlO_2 -terminated surface has an energy above $130 \text{ meV}/\text{\AA}^2$; upon reconstruction, the energy goes down to about $100 \text{ meV}/\text{\AA}^2$ (Ref. 27).

The stability of the unreconstructed TiO_2 termination is directly related to the physics of the Mott insulator. Within the bulk of GTO, electron counting tells us that one electron is available per Ti atom, and these electrons prefer to localize on individual Ti atoms, turning them into Ti^{3+} and giving rise to the LHB. In the surface layer, only one electron is available for two Ti atoms. In a band insulator (a conventional semiconductor or oxide), this imbalance of charge would lead to unoccupied surface states close to the valence band (low in the gap), which is energetically unfavorable (and provides a strong driving force for surface reconstructions). In the Mott insulator, however, the missing electron simply leads to one of the two surface Ti atoms assuming a $4+$ valence, while the other one behaves as a Ti^{3+} , as it would in the bulk. The surface state associated with Ti^{4+} is high in energy but since it is unoccupied, it does not add any energetic cost, explaining the modest value of the surface energy.

D. Hydrogen-adatom reconstruction

Hydrogen is known to lower the surface energy of many materials,^{24,25} particularly when oxygen atoms are present in the surface

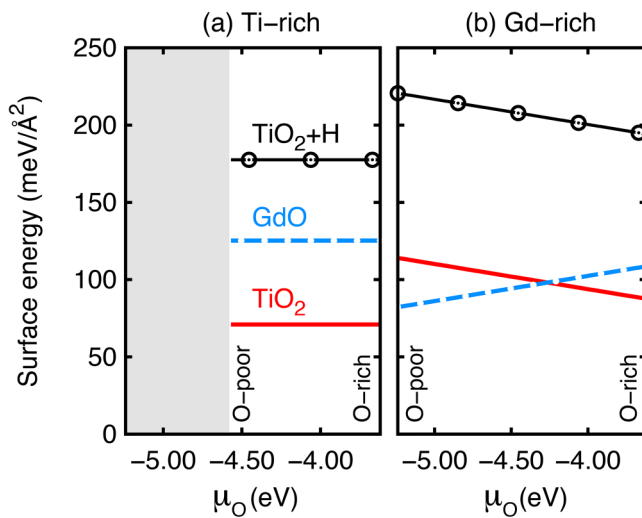


FIG. 5. Calculated surface energies (in $\text{meV}/\text{\AA}^2$) of GTO surfaces plotted as a function of μ_0 under (a) Ti-rich and (b) Gd-rich conditions. Results are shown for TiO_2 termination (solid red), GdO termination (dashed blue), and for the (1×1) H-adatom reconstruction on TiO_2 termination (open circles). Under Gd-rich conditions, the formation of competing phases of GTO restricts μ_0 to the range $-5.24 \text{ eV} \leq \mu_0 \leq -3.62 \text{ eV}$, while under Ti-rich conditions, the range, $-4.58 \text{ eV} \leq \mu_0 \leq -3.62 \text{ eV}$, is smaller (see Fig. 2). The gray shaded area in panel (a) indicates the μ_0 values for which GTO is unstable under the constraint imposed by Ti-rich conditions.

layer and strong O–H bonds can be formed.^{26,27} We, therefore, examine the stability of the TiO_2 -terminated GTO surface in the presence of hydrogen adatoms. We find the hydrogen atom is most stable in a position close to an O atom on the surface, forming a strong O–H bond [see Fig. 4(b)] with a bond length of 0.958 Å. We verified that this configuration is lower in energy than other configurations in which H bonds to a Ti atom. The H adatom donates an electron to the unoccupied surface states of the bare TiO_2 termination [see Fig. 4(a)], thus placing *both* the Ti surface atoms in a 3+ valence state. As the Ti^{4+} of the bare termination goes to a Ti^{3+} state with the addition of H, its O–Ti–O bond angles show a significant change from 94.0° and 81.9° to 95.3° and 85.1°. The bond angles for the Ti^{3+} with an unchanged valence state show only a small change, from 97.6° and 86.2° to 98.8° and 85.7°. The sum of the angles amounts to 364.9°, instead of 360°.

The surface energy of the H-adatom reconstruction, calculated using Eq. (1), is included in Fig. 5. This surface energy has the same μ_0 dependence as the bare TiO_2 termination, differing only by a term that depends on the hydrogen chemical potential μ_{H} (which was chosen to correspond to the energy of an H_2 molecule). The H-adatom reconstruction *increases* the surface energy by $107 \text{ meV}/\text{\AA}^2$ compared to the bare TiO_2 -terminated surface (see Fig. 5). Note that a more realistic choice of μ_{H} , such as equilibrium with H_2O , would raise the surface energy even higher. Our result shows that H is unlikely to bind to the TiO_2 -terminated surface and that an unreconstructed (but relaxed) polar surface is much more stable than a hydrogen-adatom reconstruction.

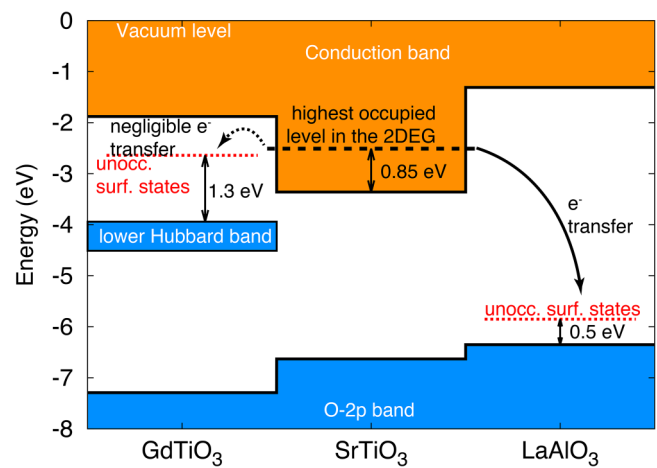


FIG. 6. Schematic illustration of charge transfer between a 2DEG in STO and the surface of either GTO (left) or LAO (right). The band alignment between GTO, LAO, and STO (from Ref. 9) is shown referenced to the vacuum level calculated for the TiO_2 -terminated GTO surface [Fig. 3(a)]. Dotted red lines show unoccupied surface state levels for the TiO_2 -terminated GTO [from Fig. 3(a)] and AlO_2 -terminated LAO surfaces (from Ref. 3). The highest occupied level in the STO 2DEG (dashed black line) was taken from Ref. 40. Electron transfer occurs from the 2DEG to low-lying LAO surface states, but the transfer to high-lying GTO surface states is far less favorable.

Considering that H is known to stabilize the surfaces of many materials,^{24–27} this result is unexpected. We can understand it, however, based on the type of bonding that occurs on the TiO_2 -terminated GTO surface and contrast it with what happens on the surfaces of conventional oxides. Oxide surfaces (e.g., LAO, Ref. 27) often have partially occupied surface states with oxygen character that lie low in the bandgap (i.e., close to the valence band, which has oxygen character). When hydrogen binds to these oxygen atoms, it supplies an electron that fills these low-lying unoccupied states, providing effective passivation of the surface. On the TiO_2 -terminated GTO surface, however, the highest occupied bands have Ti character, and the unoccupied surface states are localized on the Ti^{4+} atoms. As noted in Sec. III B, these Ti^{4+} -related surface states occur at much higher energy than the O 2p states, which are completely filled. Hydrogen can still form an O–H bond but its electron is not needed to fill an oxygen-related state; instead, it has to go into high-lying Ti states, which costs energy. It is this energy cost that makes the H-adatom reconstruction energetically unfavorable. These insights reconcile the unexpected behavior of H on the TiO_2 -terminated surface of GTO. For the GdO-terminated surface, where the Fermi level occurs much higher in energy, the energy cost of attaching an H adatom to the surface was prohibitive in our calculations.

E. Impact on the 2DEG at STO/GTO interfaces

As was discussed in the Introduction, the symmetry of stacked charged planes could also be broken at a heterointerface with a nonpolar material, and result in the formation of a high-density

2DEG at the interface. We now address the consequences for the 2DEG in an STO/GTO heterostructure when a GTO surface is present near the interface; specifically, we are interested in studying the feasibility of charge transfer between the 2DEG and GTO surface states, similar to that found to occur in the STO/LAO system for thin LAO films.³

The potential charge transfer from an interfacial 2DEG to surface states on a TiO₂-terminated GTO surface (or AlO₂-terminated LAO surface) is illustrated in Fig. 6. Electrons transfer from the highest occupied state of the 2DEG, which occurs above the CBM in STO. The highest occupied level for the full 2DEG density of $3.3 \times 10^{14} \text{ cm}^{-2}$ in STO was computed using Schrödinger–Poisson simulations, taking the effect of the field-dependent dielectric permittivity of STO into account.⁴⁰ If the 2DEG gets depleted, the highest occupied level would move closer to the CBM.

In the case of the STO/LAO heterostructure,³ a significant driving force exists for electron transfer to the surface because the unoccupied surface states on the AlO₂-terminated surface of LAO occur at very low energy on an absolute energy scale. However, the electron transfer from the interface to the surface results in a dipole that raises the energy of the surface states. For a sufficiently thick LAO layer (beyond between three and four monolayers), the energy of the surface states will align with the highest occupied level in the 2DEG in STO and some electrons will then remain at the interface. This explains the observation of a critical thickness for 2DEG formation in STO/LAO.¹⁷

In the STO/GTO system, on the other hand, the band alignment^{9,18} shows the level of the unoccupied surface states of the TiO₂ termination of GTO to occur only slightly below the highest occupied level in the 2DEG (see Fig. 6). Therefore, the energy gain due to transfer from the 2DEG to the surface states is very small, and only a small concentration of electrons will be transferred to the surface. By the same argument, in the case of a GdO-terminated GTO surface, any electrons transferred would need to go into states with energy at the UHB [Fig. 3(b)]. As the band alignment (Fig. 6) shows, the UHB occurs well above the highest occupied states of the 2DEG, which makes electron transfer impossible. The absence of lower-energy surface states in both terminations explains why the STO/GTO system exhibits the full 2DEG density, independent of the GTO thickness.

IV. CONCLUSION

We have found that the unreconstructed (001) surfaces of the Mott insulator GTO have unusually low surface energies; unreconstructed polar surfaces usually have high energies, providing a driving force for reconstructions. We attribute the stability to the ability of GTO to accommodate two valence states of Ti on the TiO₂ termination: Ti³⁺ surface atoms accommodate occupied surface states that are almost indistinguishable from the LHB, while Ti⁴⁺ atoms lead to unoccupied surface states. The surface electronic structure also explains why we find that hydrogen adatoms, which usually lead to surface passivation states, increase the surface energy.

Our conclusions about the surface stability of polar GTO surfaces are expected to be more general and applicable to other

d-band Mott insulators, such as YTiO₃ or SmTiO₃. Finally, based on the surface electronic structure, we explained why the STO/GTO interface retains the full 2DEG density that results from the polar discontinuity, whereas the STO/LAO system, where the LAO surface acts as a sink for electrons, shows a thickness-dependent 2DEG density.

ACKNOWLEDGMENTS

This work was supported by the Center for Low Energy Systems Technology (LEAST), one of six SRC STARnet Centers sponsored by MARCO and DARPA. A.J. acknowledges support from a National Science Foundation (NSF) Early Career Award (Grant No. DMR-1652994). Computational resources were provided by the Extreme Science and Engineering Discovery Environment (XSEDE), which is supported by the NSF (Grant No. ACI-1548562). Use was also made of computational facilities purchased with funds from the NSF (No. CNS-1725797) and administered by the Center for Scientific Computing (CSC). The CSC is supported by the California NanoSystems Institute and the Materials Research Science and Engineering Center (MRSEC; NSF DMR No. 1720256) at UC Santa Barbara.

DATA AVAILABILITY

The data that support the findings of this study are available within the article.

REFERENCES

- 1 A. Ohtomo and H. Y. Hwang, *Nature* **427**, 423 (2004).
- 2 A. Janotti, L. Bjaalie, L. Gordon, and C. G. Van de Walle, *Phys. Rev. B* **86**, 241108 (2012).
- 3 K. Krishnaswamy, C. E. Dreyer, A. Janotti, and C. G. Van de Walle, *Phys. Rev. B* **92**, 085420 (2015).
- 4 T. Ishihara, in *Perovskite Oxide Solid Oxide Fuel Cells*, Fuel Cells and Hydrogen Energy, edited by T. Ishihara (Springer US, Boston, MA, 2009), p. 4.
- 5 U. Diebold, *Nat. Mater.* **9**, 185 (2010).
- 6 J. A. Enterkin, A. K. Subramanian, B. C. Russell, M. R. Castell, K. R. Poeppelmeier, and L. D. Marks, *Nat. Mater.* **9**, 245 (2010).
- 7 W. Zhong, D. Vanderbilt, and K. M. Rabe, *Phys. Rev. Lett.* **73**, 1861 (1994).
- 8 C. Franchini, *J. Phys. Condens. Matter* **26**, 253202 (2014).
- 9 L. Bjaalie, B. Himmetoglu, L. Weston, A. Janotti, and C. G. Van de Walle, *New J. Phys.* **16**, 025005 (2014).
- 10 L. Bjaalie *et al.*, *Phys. Rev. B* **92**, 085111 (2015).
- 11 N. F. Mott, *Rev. Mod. Phys.* **40**, 677 (1968).
- 12 J. B. Goodenough, *J. Solid State Chem.* **3**, 490 (1971).
- 13 G. Catalan, R. M. Bowman, and J. M. Gregg, *Phys. Rev. B* **62**, 7892 (2000).
- 14 P. W. Tasker, *J. Phys. C* **12**, 4977 (1979).
- 15 M. Potthoff and W. Nolting, *Phys. Rev. B* **60**, 7834 (1999).
- 16 P. Moetakef *et al.*, *Appl. Phys. Lett.* **99**, 232116 (2011).
- 17 S. Thiel, G. Hammerl, A. Schmehl, C. W. Schneider, and J. Mannhart, *Science* **313**, 1942 (2006).
- 18 A. Janotti, L. Bjaalie, B. Himmetoglu, and C. G. Van de Walle, *Phys. Status Solidi RRL* **8**, 577 (2014).
- 19 Q. Lei *et al.*, *npj Quantum Mater.* **2**, 10 (2017).
- 20 Y. Xie, C. Bell, Y. Hikita, S. Harashima, and H. Y. Hwang, *Adv. Mater.* **25**, 4735 (2013).
- 21 J. Heyd, G. E. Scuseria, and M. Ernzerhof, *J. Chem. Phys.* **124**, 219906 (2006).
- 22 J. Heyd, G. E. Scuseria, and M. Ernzerhof, *J. Chem. Phys.* **118**, 8207 (2003).

- ²³P. Moetakef, D. G. Ouellette, J. Y. Zhang, T. A. Cain, S. J. Allen, and S. Stemmer, *J. Cryst. Growth* **355**, 166 (2012).
- ²⁴C. G. Van de Walle and J. Neugebauer, *Phys. Rev. Lett.* **88**, 066103 (2002).
- ²⁵G. Srivastava, *Appl. Surf. Sci.* **252**, 7600 (2006).
- ²⁶B. Meyer, *Phys. Rev. B* **69**, 045416 (2003).
- ²⁷K. Krishnaswamy, C. E. Dreyer, A. Janotti, and C. G. Van de Walle, *Phys. Rev. B* **90**, 235436 (2014).
- ²⁸J. Paier, M. Marsman, K. Hummer, G. Kresse, I. C. Gerber, and J. G. Angyan, *J. Chem. Phys.* **124**, 154709 (2006).
- ²⁹A. Grüneis, G. Kresse, Y. Hinuma, and F. Oba, *Phys. Rev. Lett.* **112**, 096401 (2014).
- ³⁰G. Kresse and J. Furthmüller, *Comp. Mater. Sci.* **6**, 15 (1996).
- ³¹P. E. Blöchl, *Phys. Rev. B* **50**, 17953 (1994).
- ³²G.-X. Qian, R. M. Martin, and D. J. Chadi, *Phys. Rev. B* **38**, 7649 (1988).
- ³³D. A. MacLean, H.-N. Ng, and J. Greedan, *J. Solid State Chem.* **30**, 35 (1979).
- ³⁴R. J. M. Konings *et al.*, *J. Phys. Chem. Ref. Data* **43**, 013101 (2014).
- ³⁵M. Chase, *NIST-JANAF Thermochemical Tables*, 4th ed. (American Chemical Society, Washington, D.C., 1998).
- ³⁶K. Helean, S. Ushakov, C. Brown, A. Navrotsky, J. Lian, R. Ewing, J. Farmer, and L. Boatner, *J. Solid State Chem.* **177**, 1858 (2004).
- ³⁷L. Bjaalie, A. Janotti, K. Krishnaswamy, and C. G. Van de Walle, *Phys. Rev. B* **93**, 115316 (2016).
- ³⁸K. Krishnaswamy, L. Bjaalie, B. Himmetoglu, A. Janotti, L. Gordon, and C. G. Van de Walle, *Appl. Phys. Lett.* **108**, 083501 (2016).
- ³⁹A. A. Stekolnikov, J. Furthmüller, and F. Bechstedt, *Phys. Rev. B* **65**, 115318 (2002).
- ⁴⁰H. Peelaers, K. Krishnaswamy, L. Gordon, D. Steiauf, A. Sarwe, A. Janotti, and C. G. Van de Walle, *Appl. Phys. Lett.* **107**, 183505 (2015).